ACS APPLIED MATERIALS & INTERFACES

Research Article

www.acsami.org

# Photolithographic Strategy for Patterning Preformed, Chemically Modified, Porous Silicon Photonic Crystal Using Click Chemistry

Ying Zhu,[†] Bakul Gupta,[†] Bin Guan,[†] Simone Ciampi,[†] Peter J. Reece,[‡] and J. Justin Gooding*[,†]

[†]School of Chemistry and the Australian Centre for NanoMedicine and [‡]School of Physics, University of New South Wales, Sydney 2052, Australia

Supporting Information

**ABSTRACT:** Porous silicon (PSi) is an ideal platform for label-free biosensing, and the development of porous silicon patterning will open a pathway to the development of highly parallel PSi biochips for detecting multiple analytes. The optical response of PSi photonic crystal is determined by the changes in the effective bulk refractive index resulting from reactions/events occurring within the internal pore space. Therefore, introducing precise chemical functionalities in the pores of PSi is essential to ensure device selectivity. Here we describe the fabrication of PSi patterns that possess discrete chemical functionalities that are restricted to precise locations. The key difference to previous patterning protocols for PSi is that the entire porous material is first modified with a self-assembled monolayer of a $\alpha,\omega$-diyne adsorbate prior to patterning using a microfabricated titanium mask. The distal alkyne moieties in the monolayer are then amenable to further selective modification by the archetypal "click" reaction, the copper catalyzed alkyne−azide cycloaddition (CuAAC), using the titanium mask as a resist. This type of patterning is suitable for further immobilization of biological recognition elements, and presents a new platform for highly parallel PSi biosensor for multiple detections.

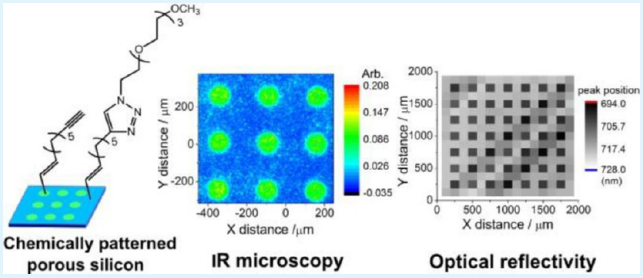


**KEYWORDS:** *porous silicon, photonic crystal, microfabrication, patterning, hydrosilylation, click reaction*

## INTRODUCTION

Porous silicon (PSi) photonic crystals are attractive material for optoelectronic and biosensing applications.[1−5] The major advantages of using PSi, as compared with other types of photonic crystal technologies, is that PSi is fabricated through a simple electrochemical etching process[6] that has a great deal of flexibility with regard to engineering the optical properties of the device. In addition, the hydride termination of as-prepared PSi can readily be modified using the well-developed hydrosilylation chemistry.[7,8] The ability to modify at will the PSi surface with monolayers enables the design of biorecognition interfaces for biosensing.[1] As an optical sensor, the response of PSi photonic crystal is determined by changes in the effective bulk refractive index resulting from reactions/events occurring within the pore space.[9,10] Chemical derivatization at precise positions of PSi is therefore an essential step for selective capture or detection of (bio)analytes.

As PSi is an ideal platform for label-free biosensing,[1] the development of PSi patterning will open a pathway to the development of highly parallel PSi biochips for detecting multiple analytes.[11] The strategies for PSi patterning fall into two categories: (i) patterning a flat silicon wafer and then forming PSi in the defined regions,[12,13] and (ii) forming a uniform PSi film first and then selectively modifying the PSi in the defined regions.[14,15] In the first strategy, a mask is first patterned on a crystalline silicon substrate, with materials such as photoresist[12,16,17] and silicon nitride.[13,18] Local anodization is then performed with the patterned silicon substrate to produce spatially defined PSi. In the second strategy, PSi structure is first formed, and then microfabrication techniques are employed for the patterning. The advantage of this second approach is that more uniform optical properties are achieved across each element of an array, because edge effects during the fabrication of the PSi caused by etching cell configuration and electrical field distribution are reduced. This method has been used for PSi micromachining for new photonic crystal structures[19,20] or uniform microparticles.[21−24] Examples of this second strategy include that of Khunget al.,[25] who reported the micropatterning of PSi films by direct laser writing, and Sweetman et al.,[15] who utilized UV light-assisted hydrosilylation to introduce two different surface functionalities to PSi with the pattern defined by a photomask. Sweetman et al.[14] have also patterned PSi using photolithography technique and silane chemistry. This latter strategy is of particular interest to the present study, as the authors pattern the surface after modifying the entire PSi structure with a base monolayer. We use a similar strategy here, but as we are interested in fabricating arrays of PSi sensors that monitor the release of protease enzymes from cells,[26] the PSi devices must be stable in biological fluids for up to several days. Hence a patterning

Received: February 15, 2013
Accepted: June 19, 2013
Published: June 19, 2013

   dx.doi.org/10.1021/am4006012 | ACS Appl. Mater. Interfaces 2013, 5, 6514−6521

approach compatible with surface chemistry that stabilizes the PSi for longer time periods than is achievable with silane chemistry is required. We have observed the greatest stabilization with thermal hydrosilylation of dialkynes.[27,28]

In the present work, we demonstrate the ability to chemically pattern PSi using microfabrication combined with surface chemistry that (1) provides unprecedented stabilization of PSi and (2) is highly compatible with further functionalization to introduce sophisticated biointerfaces into the pattern. In this approach, the entire structure was first modified with 1,8-nonadiyne by thermal hydrosilylation. The PSi substrate was then coated with titanium that was selectively removed to expose the surface chemistry in discrete regions. The attachment of further chemical functionalities to the exposed areas was achieved by copper(I)-catalyzed alkyne−azide cycloaddition (CuAAC) click reaction.[29] PSi rugate filters, with a high reflectivity stop-band within a narrow wavelength range, were employed in this work because of their demonstrated utility for biosensing.[30] This work is an important step toward the development of high-throughput, cell-based screening platforms for biosensing applications.

## EXPERIMENTAL PROCEDURE

**Fabrication of PSi Rugate Filters.** Mesoporous silicon rugate filters were prepared by galvanostatic anodization of boron-doped Si(100) wafer (highly doped wafer and medium doped wafer with resistivity 1−1.5 mΩ cm and 60−70 mΩ cm, respectively, Siltronix, France) in a 30% (v/v) hydrofluoric acid ethanolic solution.[30] The photonic structure of PSi rugate filter was designed with 40 pairs of alternative high and low refractive index layers. Etching current densities were 21.1 and 23.7 mA/cm$^2$ for the highly doped wafer, and 31.6 and 94.7 mA/cm$^2$ for the medium doped wafer. After anodization, the samples were rinsed in ethanol, dried under nitrogen gas, and stored under dry argon before further processing. The porosities of the two kinds of layer were 65.7 and 67.3% for the highly doped wafer and 54 and 72% for the medium doped wafer, which were obtained from simulation based on the Looyenga model.[31] The thickness of the PSi film from highly doped wafer was ca. 10 $\mu$m and the average pore size was ca. 45 nm, and the thickness of the PSi film from medium doped wafer was ca. 5.6 $\mu$m and the average pore size was ca. 20 nm, as determined by scanning electron microscopy.

**Modification of PSi Rugate Filters with 1,8-Nonadiyne.** Hydrosilylation of PSi samples was carried out using Schlenk line setup following a previously reported procedure.[29] Freshly etched PSi rugate filters were immersed in deoxygenated 1,8-nonadiyne in a custom-made Schlenk flask. The sample was kept under an argon atmosphere while the Schlenk flask was immersed in an oil bath with the temperature set to 170 °C for 3 h. The flask was then opened to the atmosphere, and the sample was rinsed consecutively with copious amounts of redistilled dichloromethane and ethanol, blown dry under argon, and stored under argon before use or further processing.

**Microfabrication of PSi.** The microfabrication process for coating the surface with microscale titanium patterns is shown in Scheme 1, steps a−c. The alkyne monolayer-functionalized PSi was coated with a layer of titanium at a thickness of 40 nm by thermal evaporation. The titanium-coated substrate was then processed accordting to a standard photolithographic protocol as follows. The titanium-coated PSi was covered with positive photoresist AZ6632 (Microchemicals, Germany) by spin-coating at 4000 rpm for 30 s and soft-baked at 95 °C for 5 min. The photoresist-coated substrate was irradiated with UV light for 7 s through a chrome-patterned photomask using a Quintel Q6000 mask aligner. Following UV exposure, the photoresist was immediately developed in AZMIF326 developer (Microchemicals, Germany) for 1 min, rinsed with Milli-Q water for 30 s and dried under a stream of nitrogen gas. The patterning on the photoresist was transferred to the titanium layer underneath by a wet etching process as follows. The photoresist-patterned substrate was immersed in a 5% (v/v) hydrofluoric acid in Milli-Q water for 2 s to remove the titanium layer from regions without photoresist coating, and then immediately rinsed thoroughly with Milli-Q water and dried under nitrogen gas. After the titanium patterning, the photoresist was stripped by washing the surface with copious amounts of acetone and isopropanol, and then dried under nitrogen gas.

**Scheme 1. Process for Chemical Patterning of the Internal Surface in PSi Rugate Filters**[a]

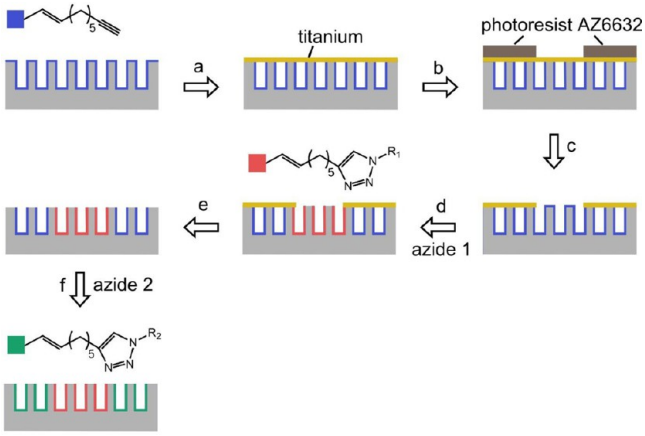


[a](a) Alkyne monolayer-modified PSi was coated with a layer of titanium by thermal evaporation; (b) titanium-coated substrate was patterned with photoresist AZ6632 by standard photolithography process; (c) patterns were transferred to titanium layer by wet etching in hydrofluoric acid aqueous solution, and the photoresist was stripped by acetone and isopropanol; (d) a first functionality was attached to the region not covered with titanium coating by a click reaction with azide **1**; (e) titanium patterns were removed by hydrofluoric acid aqueous solution; (f) a second functionality was attached to the rest region by another click reaction with azide **2**.

**Chemical Patterning of PSi Rugate Filters.** The titanium-patterned PSi rugate filter was modified with different chemical functionalities in discrete regions by click reactions (Scheme 1, steps d−f). In a typical click reaction, the following chemicals were added to a reaction tube before the alkyne-functionalized PSi sample was added: (i) azido species (10 mM, ethanol/water, 1:1), (ii) copper(II) sulfate pentahydrate (1 mol % relative to the azide), and (iii) sodium ascorbate (25 mol % relative to the azide). Click reactions were carried out at room temperature for 19 h. After the reaction, the sample was immersed in 0.5 M hydrochloric acid to remove copper on the surface, rinsed with copious amounts of water and ethanol, and dried under a stream of argon.

For the chemical patterning, the first functionality was attached to the region not coated with titanium layer by a click reaction with the first azide (azide **1** in Scheme 1). Following that, the titanium patterning was removed from the surface by the same procedure of titanium wet etching. The second functionality was subsequently attached to the rest region that retains the alkyne functionalized surface, by means of another click reaction with the second azide (azide **2** in Scheme 1).

**Surface Characterization.** The chemically patterned substrate was characterized using a PerkinElmer Spotlight 400 FTIR Microscope. IR microscopy data was collected relative to unmodified Si(100) in reflectance mode for the highly doped sample, and in transmission mode for the medium doped sample. The IR microscopy image was recorded with a pixel size of 6.25 $\mu$m and 2 scans per pixel. The scan range for the spectra was 650−4000 cm$^{-1}$, at a resolution of 16 cm$^{-1}$.

The azido species used for IR microscopy was 4-azidophenacyl bromide for both azide **1** and azide **2** in Scheme 1.

X-ray photoelectron spectroscopy (XPS) data were acquired using an ESCALAB 220iXL spectrometer with a monochromated Al K$\alpha$

source (1486.6 eV), hemispherical analyzer, and multichannel detector. Spectra were recorded in normal emission with the analyzing chamber operating below $1 \times 10^{-9}$ mbar and selecting a spot size of ~1 $mm^2$. The incidence angle was set to 58° with respect to the analyzer lens. The resolution of the spectrometer is ca. 0.6 eV as measured from the Ag $3d_{5/2}$ signal (full width at half-maximum) with a 20 eV pass energy. Survey scans were carried out over 1100−0 eV range with a 1.0 eV step size, a 100 ms dwell time, and analyzer pass energy of 100 eV. High-resolution scans were run with 0.1 eV step size, dwell time of 100 ms, and the analyzer pass energy set to 20 eV. After background subtraction using the Shirley routine, spectra were fitted with a convolution of Lorentzian and Gaussian profiles as previously reported.[32] All energies are reported as binding energies in eV and referenced to the Si 2p signal (corrected to 99.9 eV).

**Optical Characterization.** Optical reflectivity spectra were measured in the visible and near-infrared at normal incidence using a custom-built optical arrangement. The setup incorporated a USB2000+ miniature fiber-optic spectrometer (Ocean Optics Inc.) and a fiber-coupled light source (Mikropack GmbH, Germany). The spectral resolution was 1 nm and the measurement spot size was ca. 80 μm. The optical arrangement was incorporated with a 2-axis (X-Y) automated stage (MS-2000, Applied Scientific Instrumentation). A custom software platform driven by LabVIEW (National Instruments, TA) was used to process the spectra and provide program for the automatically movement of the stage. The reflectivity data of the chemically patterned surface was collected with a specified step size relative to the center-to-center distance of the circles in the array. The peak position of each reflectivity spectrum is collected by recording the wavelength corresponding to the maximum intensity after a polynomial fitting of the peak.

The azido species used for reflectivity measurement were 13-azido-2,5,8,11-tetraoxatridecane and 11-azido-3,6,9-trioxaundecan-1-ol for azides **1** and **2** in Scheme 1, respectively.

## RESULTS AND DISCUSSION

**Microfabrication Process on PSi Substrate.** The microfabrication and chemical patterning processes are shown in Scheme 1. Freshly etched PSi was functionalized with an alkyne-terminated monolayer and then coated with a layer of titanium with a thickness of 40 nm. The purpose of the titanium coating was to prevent photoresist from penetrating into the pore space, which may prevent further chemical modification of pores.[24,33] The desired pattern was formed on top of the titanium with photoresist by a standard photolithography process, and subsequently transferred to the titanium layer by a wet etching process. Removing the photoresist from specific regions revealed the titanium; hence, it could be etched away, in these regions, to expose the alkyne-terminated surface chemistry. XPS result shows there is no titanium residue on the surface after HF wet etching, which indicates the titanium is removed completely from the PSi structures (see Figure S1 in the Supporting Information). CuAAC click reaction could be performed in the exposed locations. Thereafter, the remaining titanium was removed and a second click reaction was performed to attach different surface chemistry such that a chemical pattern was formed on the PSi surface.

Figure 1a shows an optical microscopy image of a PSi substrate coated with titanium and processed using photolithography to create an array of circular apertures; the dark regions in the image are the exposed PSi substrate and the bright regions are the titanium-coated regions. The regions around the circular apertures are henceforth referred to as the background region. The diameter of the circles is 100 μm and the center-to-center distance is 250 μm. Figure 1b shows a higher-magnification image of the array where the detail of the

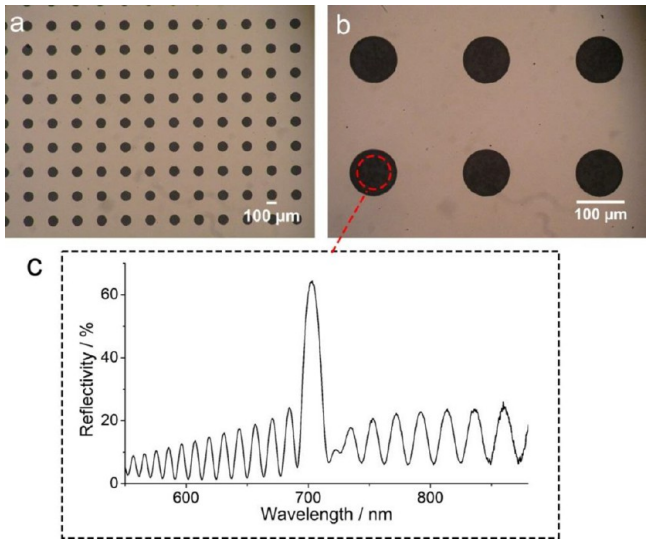


**Figure 1.** Optical microscopy images of the PSi substrate coated with titanium patterning of an array of circular apertures in (a) low magnification and (b) high magnification. (c) Reflectivity spectrum of the exposed PSi in the circular region.

patterning can be observed. It is clear that the patterning from the photomask has been faithfully reproduced, and hence the underlying porous substrate has not significantly compromised the fidelity of the microfabrication process on this size-scale.

The unknowns in the strategy in Scheme 1 are whether the surface chemistry will withstand the different processing steps. This is because the processing requires, heat, HF, and possibly UV light. Hydrosilylation chemistry has been shown to be as stable as any monolayer chemistry,[34] and able to withstand a range of extreme conditions such as strong acids and bases[35] and HF.[36] Evidence for the stability under temperatures up to 250 °C has been reported by Faucheux et al.[37] As for UV decomposition of the surface chemistry, studies by Shirahata et al.[38] and Uosaki et al.[39] highlight UV light as the most likely cause of any degradation of the surface chemistry. To assess the effect of the microfabrication process on the optical properties of the PSi film, reflectivity spectra at different steps within the processing were compared. The spectrum of a rugate filter consists of high-frequency small amplitude interference fringes and a single narrow-band high reflectivity Bragg peak, which corresponds to the characteristic optical thickness of the photonic structure. Figure 1c displays a representative reflectivity spectrum in the circular region where underneath is the exposed PSi substrate, and the peak position of this spectrum is 702.8 nm. Any material entering the pore space can be ascertained via a shift in the peak maxima.[1] Before the microfabrication process, the average peak position of the alkyne functionalized PSi film was 707.7 ± 4.6 nm (average ± standard deviation). After the processing, the reflectivity data of PSi in different exposed regions were measured, and the average peak position was 702.6 ± 2.8 nm (average ± standard deviation). This difference is within the uncertainty in peak position across a fabricated piece of PSi. Importantly, the minor shift in the reflectivity peak position indicates material used in the microfabrication process (titanium or photoresist) did not remain in the pores after the HF wet etching, as this higher refractive index of these materials, relative to air, would cause a red shift. Hence it appears that the patterning has a minimal influence on the internal surface of PSi.

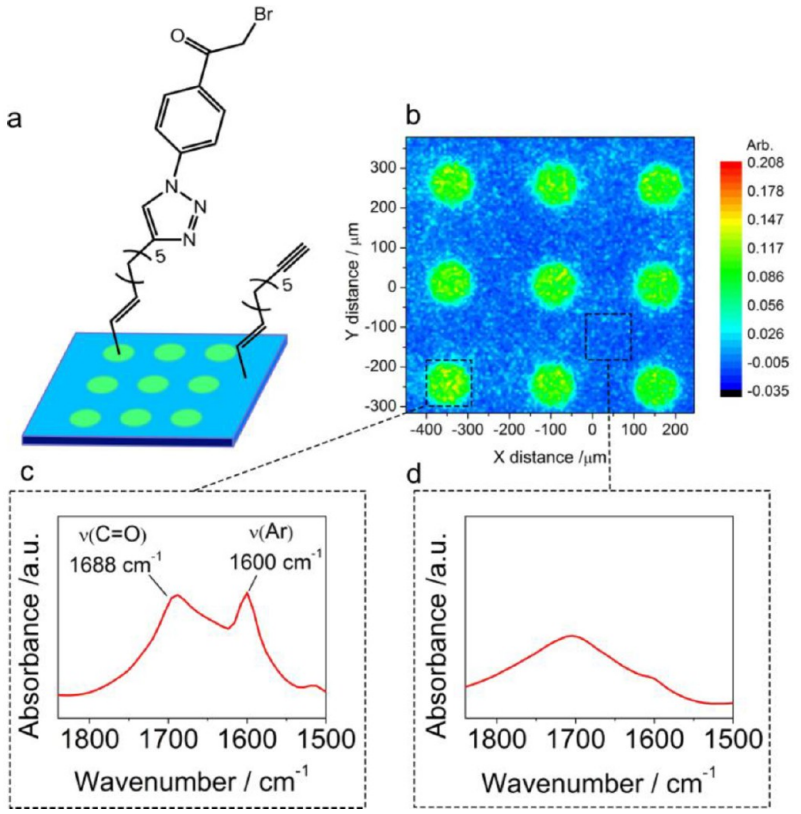


**Figure 2.** IR microscopy data of chemically patterned PSi after the first click reaction on the circular regions using 4-azidophenacyl bromide. (a) Chemistry distribution of the patterned PSi from where the IR maps were obtained; (b) IR map of the patterned PSi relative to $\nu$(Ar) mode; (c) IR spectra of the circular features in the wavenumber range including $\nu$(C═O) and $\nu$(Ar); (d) IR spectra of the background region in the same wavenumber and absorbance ranges as c.

To provide a cleaner IR spectra for interpretation of the surface chemistry, porous silicon was fabricated from medium doped Si(100) wafer. The porous silicon was modified with 1,8-nonadiyne and performed with the same titanium coating and removing processing as it is for the patterning. FTIR spectra before and after the removal of the titanium layer show no changes in the intensity of the $\nu$(C≡CH) mode at 3310 $cm^{-1}$ (see Figure S2 in the Supporting Information). The result indicates that the Ti processing has no influence on the alkyne-terminated monolayer, and the surface can be further modified by click chemistry.

**Chemical Patterning Measured by IR Microscopy.** Initially, the chemical patterning was prepared using 4-azidophenacyl bromide for the CuAAC click reaction. A first click reaction with 4-azidophenacyl bromide (see structure 1 in Table S1 in the Supporting Information) was performed on the circular regions, and the titanium coating was removed afterward. XPS shows there is no copper(I) residue after the click reaction, which might be toxic (see Figure S3 in the Supporting Information). Figure 2a shows a schematic of the chemistry distribution after the titanium removal. IR microscopy was used to characterize the chemically patterned PSi. As generally observed for PSi photonic crystals, the reflectance-FTIR spectrum was composed of an interference fringe arising from reflection at the air−PSi and PSi−Si interface and the monolayer characteristics[40] (see Figure S4 in the Supporting Information). Therefore, 4-azidophenacyl bromide was chosen as the aryl group was a strong IR marker.[9] Panels c and d in Figure 2 display representative IR spectra acquired within the circular features and the background region, respectively. In the case of the background region, the titanium has now been removed. In the circular features, a $\nu$(C═O) stretching mode at 1688 $cm^{-1}$ and $\nu$(Ar) mode at 1600 $cm^{-1}$ are apparent, whereas the background does not exhibit these absorbance bands. Figure S4 in the Supporting Information shows the IR spectra from 1200 $cm^{-1}$ to 4000 $cm^{-1}$ in the background region and circular region. Figure 2b displays the IR map of a 700 × 700 $\mu m^2$ area of the chemically patterned PSi relative to the area of the $\nu$(Ar) mode. The IR map shows that the circular features have a significantly higher intensity in $\nu$(Ar) than the background region. Figure S5 in the Supporting Information shows the IR map relative to $\nu$(C≡CH) mode at 3310 $cm^{-1}$, where the background region has a higher intensity in $\nu$(C≡CH) than the circle regions, which suggests a disappearance of the alkyne in the circle regions. Both the IR maps and the spectra indicate that the azido species is attached on the circular regions by the first click reaction.

To demonstrate that the patterning is not due to physical adsorption or oxidation, a control experiment was performed with all the same reagents required for the click reaction, with the exception of copper(II) sulfate, which becomes the source of copper(I) for the catalysis of the reaction. Both IR microscopy and optical reflectivity were used to characterize the surface after the titanium removal. Figure S6 in the Supporting Information shows the IR map relative to the area of $\nu$(Ar) mode, and there is no pattern over the surface, which suggests the click reaction can only proceed for the surface in the presence of copper(I) and that there is no physical adsorption on the surface. Optical reflectivity also shows there is no shift at the same circle regions before and after the


dx.doi.org/10.1021/am4006012 | ACS Appl. Mater. Interfaces 2013, 5, 6514−6521

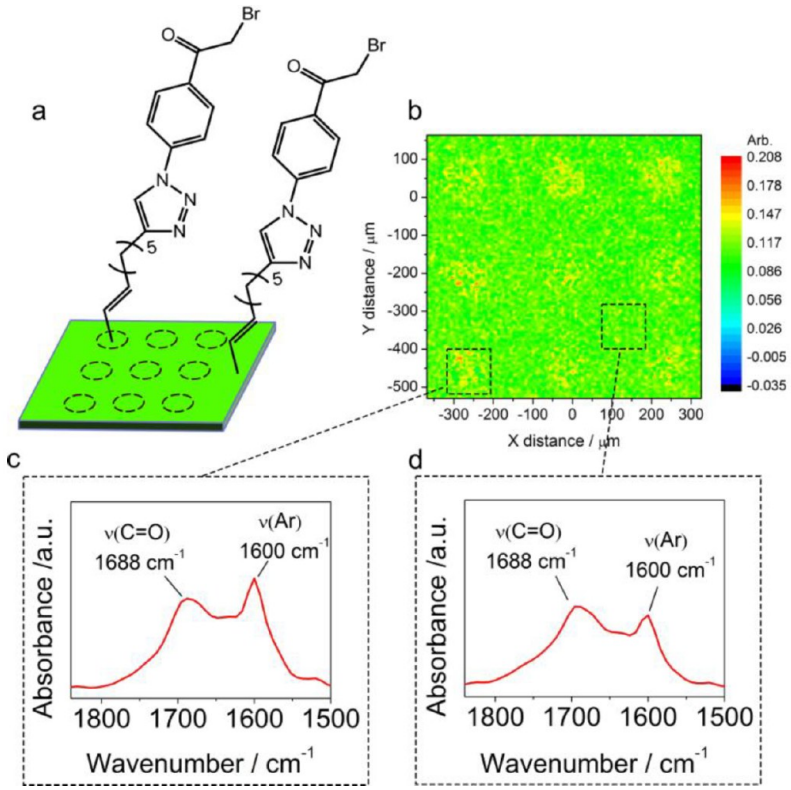


**Figure 3.** IR microscopy data of PSi after the second click reaction on the background regions using 4-azidophenacyl bromide. (a) Chemistry distribution of the PSi from where the IR maps were obtained; (b) IR map of the PSi relative to $\nu$(Ar) mode; (c) IR spectra of the circular feature in the wavenumber range including $\nu$(C═O) and $\nu$(Ar); (d) IR spectra of the background region in the same wavenumber and absorbance ranges as c.

processing, which indicates little or no oxidation occurs that might lead to the patterning (see Table S2 in the Supporting Information).

The same chemistry patterning as shown in Figure 2 was also performed on the porous silicon from medium-doped Si(100). The circular region was modified by click reaction using 4-azidophenacyl bromide, and the background region retains the alkyne functionality. The spectra in the circular region shows an apparent decrease in $\nu$(C≡CH) mode at 3310 $cm^{-1}$ and the appearance of triazole rings with an $\omega$-ring vibration at 1520 $cm^{-1}$ (see Figure S7 in the Supporting Information). The results confirmed that the click chemistry is actually occurring for the patterning.

To provide evidence that the unmodified area with the alkyne monolayer can be further functionalized with azido species, a second click reaction with the same azido species, 4-azidophenacyl bromide, was performed on the same PSi sample after the measurements presented in Figure 2. Figure 3a shows a schematic of the chemistry distribution after the second click reaction. Panels c and d in Figure 3 display the IR spectra of the circular features and the background region, where both the regions show the appearance of $\nu$(C═O) mode at 1688 $cm^{-1}$ and $\nu$(Ar) mode at 1600 $cm^{-1}$. This result indicates that the background region has been successfully modified with the azido species. Figure 3b displays the IR map of a 700 × 700 $\mu m^2$ area of the PSi relative to the area of $\nu$(Ar) mode. It can be seen that the same functional groups are present in the background region after the second click reaction, although there is a slight difference in the intensity of aryl group on different regions. The maps and the spectra show that background region is also modified with azido species by click reaction. The result from the IR microscopy suggests that discrete regions of PSi can be modified with chemical functionalities separately and that further coupling of chemical functionalities of the base alkyne-terminated monolayer are not deleteriously affected by the processing steps required in the patterning process.

**Chemical Patterning Measured by Optical Reflectivity.** As the fabricated PSi is a photonic crystal, the attachment of monolayers onto the internal surface can be confirmed via a red shift of the reflectivity peak. The azido species with tetra(ethylene glycol) ($EO_4$) moiety were used in this case, so that the surface can be patterned with an antifouling layer that also provides a coupling point for future biomolecule patterning.[41] In this case, titanium was left on the circular regions and removed from the background regions. A first CuAAC click reaction was performed with 13-azido-2,5,8,11-tetraoxatridecane (see structure 2 in Table S1 in the Supporting Information) to the background regions, so as to provide an antifouling property with an inert distal group with a view to applications as cell-based biosensors. Thereafter, the titanium coating was removed from the circular regions, and the substrate was characterized by reflectivity measurement incorporated with a XY automated stage. Figure 4a shows a schematic of the chemistry distribution after the titanium removal. The measurement scanning was performed in an array format with the step size of 125 $\mu$m, which is half of the center-to-center distance of the circles in the array. In this case, the stage was moved to defined locations such that reflectivity spectra of each circular region, as well as spectra of the background between each circular region, were recorded. Figure 4b presents a gray scale map of the reflectivity peak position distribution after the first click reaction. Figure 4c shows representative reflectivity spectra in one circular region

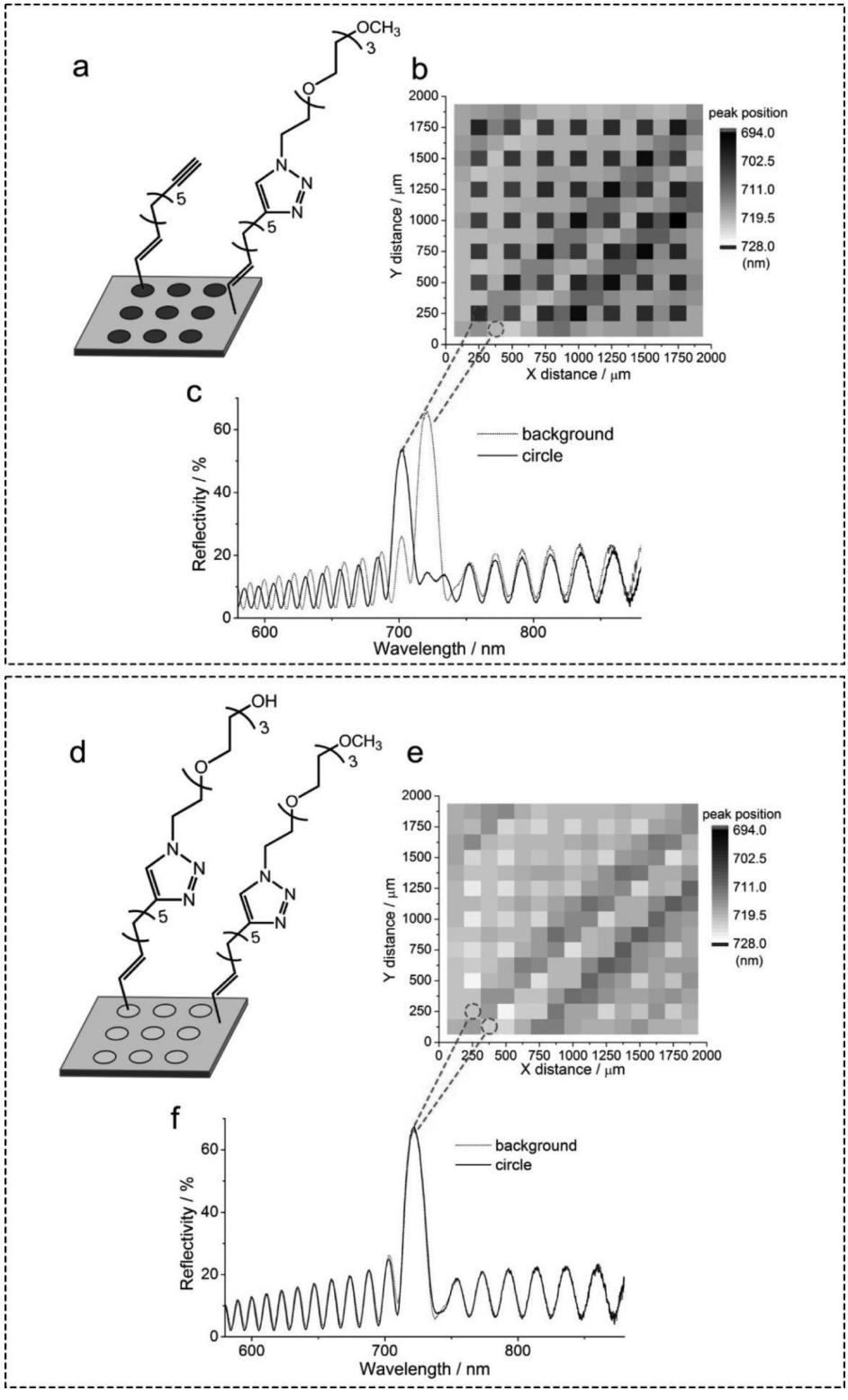


**Figure 4.** Optical reflectivity data of PSi rugate filter. (a) Chemistry distribution on PSi film after the first click reaction on the background regions using 13-azido-2,5,8,11-tetraoxatridecane; (b) the gray scale map of the reflectivity peak position distribution from a; (c) reflectivity spectra in one circle region and one background region from a. (d) Chemistry distribution of the PSi after the second click reaction on the circular regions using 11-azido-3,6,9-trioxaundecan-1-ol; (e) the gray scale map of the reflectivity peak position distribution from d; (f) reflectivity spectra in one circle region and one background region from d.

and one background region, with the corresponding peak positions 702.1 and 720.5 nm, respectively. It can be seen from Figure 4b that in the background region the peaks were at longer wavelengths than the circular features on average so that a gray scale pattern appears on the map. The peak position difference indicates that the background has been functionalized with the azide species. The contrast in the background alone was due to minor amounts of heterogeneity in the PSi


dx.doi.org/10.1021/am4006012 | ACS Appl. Mater. Interfaces 2013, 5, 6514−6521

film optical thickness resulted in the electrochemical etching process.

After the first measurement, the substrate was subsequently modified via a second reaction with 11-azido-3,6,9-trioxaundecan-1-ol (see structure 3 in Table S1 in the Supporting Information), which is to provide an antifouling moiety terminated with a hydroxyl group that can be further activated to immobilize biomolecules. Figure 4d shows a schematic of the chemistry distribution after the second click reaction. The substrate was scanned again by reflectivity measurement at the same individual positions and step size. Figure 4e displays a gray scale map of the reflectivity peak position after the second click reaction. Figure 4f shows representative reflectivity spectra in one circular region and one background region, with the corresponding peak positions 721.2 and 720.5 nm, respectively. It can be seen from Figure 4e that the peak position of the circular features red-shifted to longer wavelengths, and the contrast in the map drastically reduced. The diminution in the contrast between the circular regions and the background indicates that the second azide species has been attached to the circular regions.

Figure 5 shows the distribution of the peak wavelength shifts of individual measured positions in the two different regions

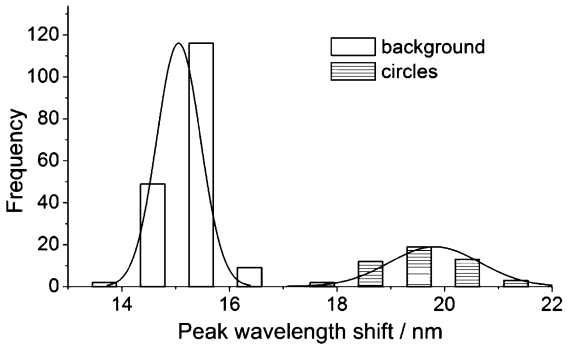


**Figure 5.** Histogram of peak wavelength shifts of individual measured positions in the two different regions after the click reactions with $EO_4$ species.

after the respective modifications. There is a 15.1 ± 0.4 nm (average ± standard deviation) red shift in the background regions and 19.8 ± 0.8 nm (average ± standard deviation) red shift in the circular regions. The ~4.7 nm difference between the two different regions indicates the microfabrication process has a small influence on the coupling yield of the surface chemistry that leads to the minor difference in the red shifts. It is noteworthy that the measurements are fixed in each individual position before and after modification, which makes the peak shift of each measurement much more reliable than that measured from PSi film without an array format. Table S3 in the Supporting Information summarizes the reflectivity data of both regions before and after the respective modifications. The result of optical reflectivity indicates that the click reaction was successfully achieved in both regions in this sequential modification process represented in Scheme 1. The reflectivity measurement for the microarray is an important characterization method for the development of highly parallel PSi-based optical biosensor.

## CONCLUSION

We have demonstrated a generic approach to introduce different functional groups in discrete regions of the internal surface of PSi photonic crystal. PSi substrate modified with alkyne-terminated monolayers was coated with microscale titanium patterns using microfabrication processes of metal deposition, photolithography, and metal wet etching. Different functionalities were subsequently attached to the internal surface of PSi in the regions defined by the titanium mask using click reactions. Characterization methods of IR and reflectivity measurement were used to obtain information regarding the monolayer and subsequent further modification via click chemistry on the pore surface. This approach can also potentially be applied to other porous materials using different modification strategies. As the optical sensing ability of PSi is determined by the refractive index change in the bulk structure, this work of PSi chemical patterning of the internal surface may lead to the development of highly parallel PSi biosensors for multiple detections.

## ASSOCIATED CONTENT

### Supporting Information

Molecule structures used in the work; additional IR maps and spectra, XPS result, and optical reflectivity data. This material is available free of charge via the Internet at http://pubs.acs.org.

## AUTHOR INFORMATION

### Corresponding Author

*E-mail: justin.gooding@unsw.edu.au.

### Notes

The authors declare no competing financial interest.

## ACKNOWLEDGMENTS

The authors thank the Australian Research Council (DP110102183), NHMRC (project grant APP1024723) and the NSW Node of the Australian National Fabrication Facility for support.

## REFERENCES

(1) Kilian, K. A.; Böcking, T.; Gooding, J. J. *Chem. Commun.* **2009**, 630−640.
(2) Sailor, M. J.; Wu, E. C.. *Adv. Funct. Mater.* **2009**, *19*, 3195−3208.
(3) Bisi, O.; Ossicini, S.; Pavesi, L. *Surf. Sci. Rep.* **2000**, *38*, 1−126.
(4) Stewart, M. P.; Buriak, J. M. *Adv. Mater.* **2000**, *12*, 859−869.
(5) Bailey, R. C.; Parpia, M.; Hupp, J. T. *Mater. Today* **2005**, *8*, 46−52.
(6) Lehmann, V.; Stengl, R.; Luigart, A. *Mater. Sci. Eng., B* **2000**, *B69−70*, 11−22.
(7) Gooding, J. J.; Ciampi, S. *Chem. Soc. Rev.* **2011**, *40*, 2704−2718.
(8) Buriak, J. M. *Chem. Rev.* **2002**, *102*, 1271−1308.
(9) Guan, B.; Ciampi, S.; Le Saux, G.; Gaus, K.; Reece, P. J.; Gooding, J. J. *Langmuir* **2011**, *27*, 328−334.
(10) Kilian, K. A.; Böcking, T.; Gaus, K.; Gooding, J. J. *Angew. Chem., Int. Ed.* **2008**, *47*, 2697−2699.
(11) Jane, A.; Dronov, R.; Hodges, A.; Voelcker, N. H. *Trends Biotechnol.* **2009**, *27*, 230−239.
(12) Flavel, B. S.; Sweetman, M. J.; Shearer, C. J.; Shapter, J. G.; Voelcker, N. H. *ACS Appl. Mater. Interfaces* **2011**, *3*, 2463−2471.
(13) Chiappini, C.; Tasciotti, E.; Fakhoury, J. R.; Fine, D.; Pullan, L.; Wang, Y.-C.; Fu, L.; Liu, X.; Ferrari, M. *ChemPhysChem* **2010**, *11*, 1029−1035.
(14) Sweetman, M. J.; Shearer, C. J.; Shapter, J. G.; Voelcker, N. H. *Langmuir* **2011**, 9497−9503.

(15) Sweetman, M. J.; Ronci, M.; Ghaemi, S. R.; Craig, J. E.; Voelcker, N. H. *Adv. Funct. Mater.* **2012**, *22*, 1158−1166.
(16) Chen, L.; Chen, Z.-T.; Wang, J.; Xiao, S.-J.; Lu, Z.-H.; Gu, Z.-Z.; Kang, L.; Chen, J.; Wu, P.-H.; Tang, Y.-C.; Liu, J.-N. *Lab Chip* **2009**, *9*, 756−760.
(17) Cunin, F.; Schmedake, T. A.; Link, J. R.; Li, Y. Y.; Koh, J.; Bhatia, S. N.; Sailor, M. J. *Nat. Mater.* **2002**, *1*, 39−41.
(18) Rea, I.; Lamberti, A.; Rendina, I.; Coppola, G.; Gioffre, M.; Iodice, M.; Casalino, M.; De Tommasi, E.; De Stefano, L. J. *Appl. Phys.* **2010**, *107*, 014513−4.
(19) Jamois, C.; Li, C.; Orobtchouk, R.; Benyattou, T. *Photonics Nanostruct.* **2010**, *8*, 72−77.
(20) Li, C.; Orobtchouk, R.; Benyattou, T.; Belarouci, A.; Chevolot, Y.; Monnier, V.; Souteyrand, E.; Gerelli, E.; Jamois, C. In *Biosensors: Emerging Materials and Applications*; Serra, P. A., Ed.; InTech: Rijeka, Croatia, 2011, p 265.
(21) Meade, S. O.; Sailor, M. J. *Phys. Status Solidi R* **2007**, *1*, R71−R73.
(22) Meade, S. O.; Chen, M. Y.; Sailor, M. J.; Miskelly, G. M. *Anal. Chem.* **2009**, *81*, 2618−2625.
(23) Adriani, G.; de Tullio, M. D.; Ferrari, M.; Hussain, F.; Pascazio, G.; Liu, X.; Decuzzi, P. *Biomaterials* **2012**, *33*, 5504−5513.
(24) Godin, B.; Chiappini, C.; Srinivasan, S.; Alexander, J. F.; Yokoi, K.; Ferrari, M.; Decuzzi, P.; Liu, X. *Adv. Funct. Mater.* **2012**, *22*, 4225−4235.
(25) Khung, Y.-L.; Graney, S. D.; Voelcker, N. H. *Biotechnol. Prog.* **2006**, *22*, 1388−1393.
(26) Kilian, K. A.; Lai, L. M. H.; Magenau, A.; Cartland, S.; Böcking, T.; Di Girolamo, N.; Gal, M.; Gaus, K.; Gooding, J. J. *Nano Lett.* **2009**, *9*, 2021−2025.
(27) Guan, B.; Magenau, A.; Kilian, K. A.; Ciampi, S.; Gaus, K.; Reece, P. J.; Gooding, J. J. *Faraday Discuss.* **2011**, *149*, 301−317.
(28) Ciampi, S.; Eggers, P. K.; Le Saux, G.; James, M.; Harper, J. B.; Gooding, J. J. *Langmuir* **2009**, *25*, 2530−2539.
(29) Ciampi, S.; Böcking, T.; Kilian, K. A.; Harper, J. B.; Gooding, J. J. *Langmuir* **2008**, *24*, 5888−5892.
(30) Ilyas, S.; Böcking, T.; Kilian, K.; Reece, P. J.; Gooding, J.; Gaus, K.; Gal, M. *Opt. Mater.* **2007**, *29*, 619−622.
(31) Squire, E. K.; Snow, P. A.; St. Russel, P.; Canham, L. T.; Simons, A. J.; Reeves, C. L. *J. Lumin.* **1999**, *80*, 125−128.
(32) Ciampi, S.; Böcking, T.; Kilian, K. A.; James, M.; Harper, J. B.; Gooding, J. J. *Langmuir* **2007**, *23*, 9320−9329.
(33) Arens-Fischer, R.; Krüger, M.; Thönissen, M.; Ganse, V.; Hunkel, D.; Marso, M.; Lüth, H. J. *Porous Mater.* **2000**, *7*, 223−225.
(34) Ciampi, S.; Harper, J. B.; Gooding, J. J. *Chem. Soc. Rev.* **2010**, *39*, 2158−2183.
(35) Boukherroub, R.; Morin, S.; Bensebaa, F.; Wayner, D. D. M. *Langmuir* **1999**, *15*, 3831−3835.
(36) Song, J. H.; Sailor, M. J. *Comments Inorg. Chem.* **1999**, *21*, 69−84.
(37) Faucheux, A.; Yang, F.; Allongue, P.; de Villeneuve, C. H.; Ozanam, F.; Chazalviel, N. J. *Appl. Phys. Lett.* **2006**, *88*, 193123−3.
(38) Shirahata, N.; Yonezawa, T.; Seo, W.-S.; Koumoto, K. *Langmuir* **2004**, *20*, 1517−1520.
(39) Uosaki, K.; Quayum, M. E.; Nihonyanagi, S.; Kondo, T. *Langmuir* **2004**, *20*, 1207−1212.
(40) Böcking, T.; Kilian, K. A.; Reece, P. J.; Gaus, K.; Gal, M.; Gooding, J. J. *Soft Matter* **2012**, *8*, 360−366.
(41) Le Saux, G.; Magenau, A.; Böcking, T.; Gaus, K.; Gooding, J. J. *Plos One* **2011**, *6*, e21869.